Heliyon 7 (2021) e06793

Contents lists available at ScienceDirect

Heliyon

journal homepage: www.cell.com/heliyon

Research article

A compact dual-band Dolly-shaped antenna with parasitic elements for automotive radar and 5G applications

Ce Lakpo Bamy [a,*], Franck Moukanda Mbango [b], Dominic Bernard Onyango Konditi [c], Pierre Moukala Mpele [a]

[a] Department of Electrical Engineering, Pan African University Institute of Basic Sciences Technology and Innovation (PAUSTI), Juja, Kenya
[b] Faculty of Sciences and Techniques, Electrical and Electronics Engineering Laboratory, Marien Ngouabi University, B.P 69, Brazzaville, Congo
[c] School of Electrical and Electronics Engineering, Technical University of Kenya (TUK), 52428-00200, Nairobi, Kenya

ARTICLE INFO

Keywords:
Automotive radar
5G
ISM applications
Dual-band antenna
Parasitic elements

ABSTRACT

In this paper, a compact dual-band Dolly-shaped antenna (DBDSA), resonating at 23.52 GHz and 28.39 GHz, is proposed for automotive radar, 5G, and Industrial, Scientific, and Medical (ISM) applications. The antenna is designed on a $7 \times 7 \times 1.28$ mm^3 which is $0.541\lambda_0 \times 0.541\lambda_0 \times 0.099\lambda_0$ in electric size, where λ_0 represents the free space wavelength at 23.16 GHz. Rogers RO3010 substrate with a dielectric constant of 10.2 and a loss tangent is about 0.0022 has been used. Two F-shaped parasitic elements and a rectangular slot have been used to achieve the desired electromagnetic antenna performances. After modeling and optimizing the proposed antenna configuration through High-Frequency Structure Simulator (HFSS) software, its prototype was manufactured and measured to validate the simulated results. The DBDSA achieves an overall radiation efficiency of 80% within the two operating frequency bands. The radar band exhibits a stable gain of 5.51 dBi, while the 5G band has a gain of 4.55 dBi. Furthermore, the experimental results show that the $|S_{11}| \leq$-10 dB bandwidths are 1.16 GHz (23.16 GHz–24.32 GHz) in the lower band and 634 MHz (28.078 GHz–28.712 GHz), respectively. A good agreement is found between the simulated and measured results.

1. Introduction

The millimeter wave technologies have attracted a lot of researchers from both industries and academia. Due to its attractive properties such as large bandwidth, miniaturization of RF front end including antennas, high resolution, and low interference, the mm-wave spectrum (30–300 GHz) is considered as the potential candidate for high-speed communication services in 5G networks [1]. For 5G antennas in one hand, high gain, low profile, low cost, broadband or multiband operation, multiploidization, and specific radiation direction are among several design parameters that have higher priorities than others [2]. Moreover, 5G networks are emerging as the foundation for advanced communication services and as the infrastructure supporting socio-economic development and driving industrial digital transformation [3]. The frequency bands centered at 28, 38, 60, and 73 GHz have been allocated for 5G mobile communications by International Telecommunications Union (ITU) [4]. Various types of planar antenna solutions for 5G communication systems have been developed over the past decade. Those antennas are either based on a single radiating element [5, 6, 7], MIMO or phased array antenna systems [8, 9]. The antennas based on MIMO technology despite their capabilities to improve the performance of the latter, have some drawback such as mutual coupling effect, surface wave and spurious waves as well as adequate techniques to solve those issues [10, 11, 12, 13, 14].

On the other hand, with increasing traffic density and road accidents, an increasing interest has emerged for additional electronic vision to improve comfort and safety. This includes closed-circuit television (CCTV), infrared sensors, laser, and radar [15]. As the core sensors of driver assistance systems, automotive radars can be broadly split into three categories: short range (SRR, up to a few 10 m) for parking aid, obstacle and pedestrian detection, medium-range (MRR, about 40–100 m) for cross-traffic alert and lane change assist, and long-range (LRR, up to 200 m or even 250 m) for Adaptive Cruise Control [16, 17, 18]. As for 5G antennas, automotive radar antennas require small size and depth for vehicle integration, high gain, and cost-effectiveness [19, 20]. The antenna proposed in [21] employs MIMO technology for the development of automotive radar for adaptive cruise control (ACC) and automatic emergency braking (AEB) in Moreover, a 12×8 antenna array designed at 24

* Corresponding author.
E-mail address: bamyeric@gmail.com (C.L. Bamy).

https://doi.org/10.1016/j.heliyon.2021.e06793
Received 23 February 2021; Received in revised form 4 April 2021; Accepted 9 April 2021

GHz for automotive radar used for blind spot detection (BSD), Lane change assistance (LCA), and rear cross-traffic alert (RCTA) [22]. To meet the different needs of modern mobile communication, vehicles are loaded with various functional antennas, which can be used in emergency call, entertainment, navigation and positioning [23]. A significant amount of research has provided numerous MIMO and phased array antennas designs for automotive radar and 5G applications. However, multiple antennas in a confined space result into other issues such as mutual coupling or isolation between radiating elements [24]. Consequently, some recent works propose single element antennas for the same applications. For instance, in [25], a single element W-band plumb shaped patch antenna has been proposed for automotive radar and 5G applications. Similarly, in [26] an ultra-wideband mm-wave antenna for automotive radar and 5G applications is presented in the frequency range 16–40 GHz. In [27], another single element antenna is investigated for use in automotive radar and 5G applications. A rectangular shape is used, and the antenna exhibits 5.64 dB gain in its upper operating frequency band.

The antenna performance can be enhanced or degraded by the feeding technique, the parasitic patch elements, the defective ground structure, the slot, the air gap, the shorting pin, and the metamaterial [28, 29, 30]. From the literature, the parasitic element has two interesting features that can be exploited in antenna design engineering. Its helps in either generating a resonant frequency or enhancing the performances of the planar antennas [31, 32, 33]. Furthermore, the combination of automotive radar and 5G technologies has not yet attracted more researchers despite few works done.

This work proposes a novel antenna solution for automotive mobile communications and radar applications. This is to not only to maintain the devices miniaturized but also to prove the possibilities of using different applications by a single device. In the remaining part of this paper, the proposed antenna design methodology based on mathematical model is presented before discussing the simulated and measured results.

2. Antenna design

2.1. Antenna configuration

The proposed Dolly-shaped antenna (DSDBA) is designed on a single-layered substrate with an overall volumetric size of $7 \times 7 \times 1.28$ mm^3, corresponding to an electric size of $0.541\lambda_0 \times 0.541\lambda_0 \times 0.099\lambda_0$ where λ_0 represents the free space wavelength at 23.16 GHz. The radiating patch is printed on a Rogers RO3010 substrate with a dielectric permittivity (ε_r) of 10.2 and a loss tangent of 0.0022. The analysis of the proposed Dolly-shaped antenna has been performed using HFSS software. Two F-shaped parasitic elements and a rectangle slot of 3 mm^2 have been added to the antenna design structure to achieve the desired performance. The geometry of the proposed antenna design is presented in Figure 1. All the optimized antenna design parameters are listed in Table 1.

2.2. Mathematical modeling

By using the broadband planar monopole antennas principle described in [34, 35] and considering the above-given data in Table 1, the radiating total active area of the radiating element is equated to that of the equivalent cylindrical monopole antenna, yielding to.

$$2\pi rL = S \tag{1}$$

where L and r denote the length and the radius of the equivalent cylindrical monopole antenna and S the patch's surface.

Based on the geometry of the antenna, the surface of the proposed Dolly-shaped configuration is determined by:

$$S = 2\pi\left(R_2{}^2\right) + 0.425\pi\left(R_1{}^2\right) + \pi\ R_1{}^2 + 0.75\pi R_{C1}{}^2 + \pi R_{C2}{}^2 \tag{2}$$

The length of the equivalent cylindrical monopole antenna can be determined using the following formula:

$$L = R_2 + 2R_1 + R_{C1} + \frac{1}{4}R_{C2} \tag{3}$$

From Eqs. (1) and (2), the radius r of the equivalent cylindrical monopole antenna is given as:

$$r = \frac{S}{2\pi L} \tag{4}$$

The width will be calculated using this formula:

$$W = 4 \times R_2 + 0.425 \times R_1 \tag{5}$$

where W is the width of the patch.

The frequency of resonance of the lower band is therefore computed as per the following in [35]:

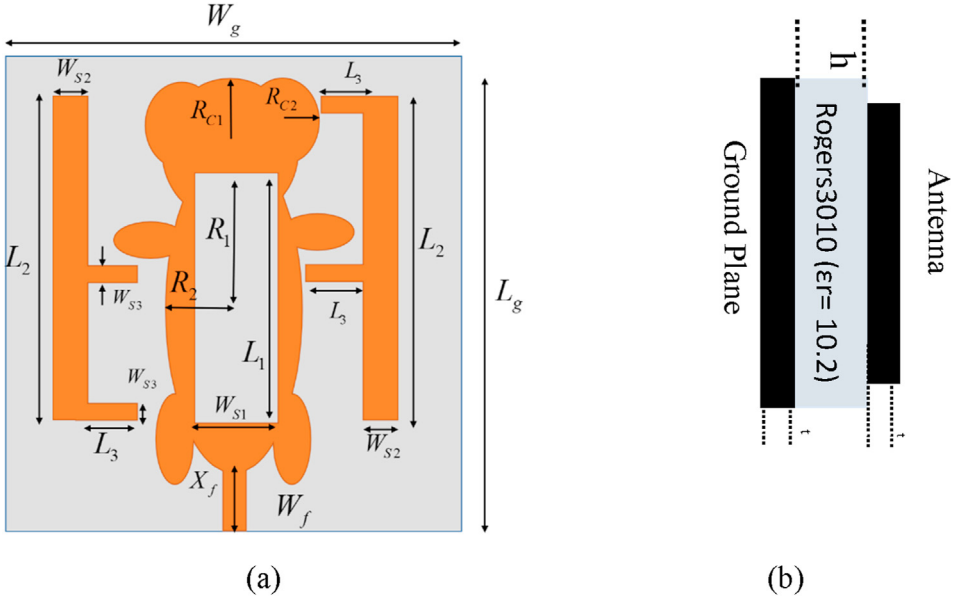

Figure 1. Geometry of the antenna: (a) top view, (b) side view.

Table 1. Design parameters of the proposed antenna.

Parameters	Description	Value
W_g	Width of the ground plane	7 mm
L_g	Length of the ground plane	7 mm
S	The surface of the radiating element	7.053 mm^2
X_f	Length of the feedline	3.1255 mm
W_f	Width of the feedline	0.5 mm
L_1	Length of the slot of the radiating element	3 mm
Ws_1	Width of the slot of the radiating element	1 mm
L_2	Length of the parasite element 1	5 mm
Ws_2	Width of the parasite element 1	0.5 mm
Ws_3	Length of the parasite element 2	0.25 mm
Ws_2	Width of the parasite element 2	0.25 mm
Rc_1	The radius of the big circle	2 mm
Rc_2	The radius of the small circle	0.5 mm
R_1	The major axis of the big ellipse	1 mm
R_2	The Major axis of the small ellipse	0.5 mm
R_3	The minor axis of the big ellipse ($R_3 = r_1 \times R_1$)	0.425 mm
R_4	The minor axis of the small ellipse ($R_4 = r_2 \times R_2$)	0.25 mm
r_1	The ellipticity ratio of the big ellipses (body of the Ant.)	0.425
r_2	The ellipticity ratio of the small (hands and feet of the Ant.)	0.5

$$f_{rL} = \frac{7.2}{\sqrt[4]{\varepsilon_{eff}}(L + r + P)} \tag{6}$$

P is the gap between the length of the feed line and the big ellipse's major axis.

The effective permittivity is determined using the following formula:

$$\varepsilon_{eff} = \frac{\varepsilon_r + 1}{2} + \frac{\varepsilon_r - 1}{2}\left[1 + 12\frac{h}{W}\right]^{-0.5} \tag{7}$$

2.3. Antenna's shape effect

In order to validate the Dolly-shaped, a comparative study has been carried out. The empirical shapes with the same dimensions have been simulated in the same frequency range. The result is presented in Figure 2 below.

From Figure 2, the Dolly-Shaped antenna provides encouraging performances compared to the empirical shapes.

2.4. Effects of the parasitic elements and rectangular slot

The parasitic elements (PE) and the slot help to create multi-band behavior and enhance the antenna performance [36, 37, 38]. Figure 3 illustrates the effect of the parasitic elements and the slot on the antenna's reflection coefficient.

From Figure 3, the simulated results show that the Dolly-shape antenna (DSA) alone resonates at 24.74 GHz. By inserting a rectangular slot in the DSA, the resonant frequency is shifted rightwards from 24.74 GHz to 24.94 GHz with a better reflection coefficient as compared to the first case. Furthermore, it can be observed that by adding the two F-shaped parasitic elements on the latter, the lower resonant frequency shifted slightly leftwards from 24.74 GHz to 23.86 GHz in the lower band while creating another resonant frequency at 27.93 GHz in the antenna's upper band. Finally, combining the rectangular slot and the two F-shaped parasitic elements with the DSA yields the optimal results. The resonant frequencies are shifted from 23.86 GHz and 27.93 GHz–24.08 GHz and 28.15 GHz, respectively. Moreover, the reflection coefficients have been improved, from -20.94 dB to -44.20 dB in the lower band and -32.08 dB in the upper band.

The methodology process can be summarized into three steps, as illustrated in Figure 4:

- Design of a Dolly-shape antenna (Figure 4a)
- Insertion of two F-shape parasitic elements (Figure 4b)
- Insertion of a rectangular slot (Figure 4c)

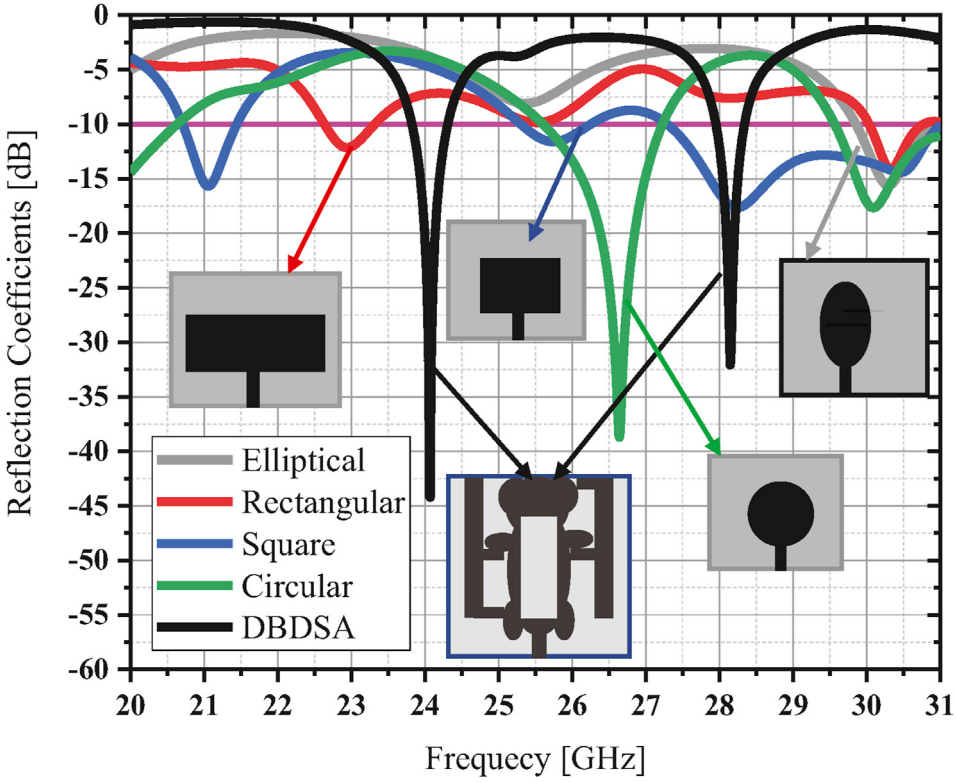

Figure 2. Comparative Study between the empirical shapes and the Dolly-Shaped.

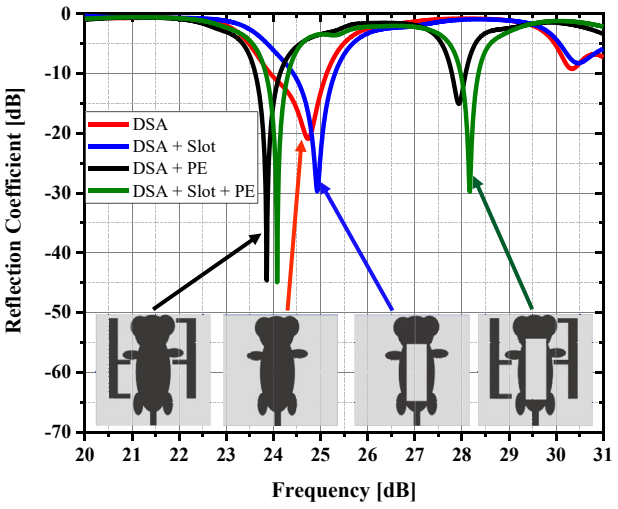

Figure 3. Comparison of the simulated reflection coefficients.

3. Result and discussion

3.1. Reflection coefficient

To combine the useful with the pleasant, the proposed DBDSA has been manufactured to validate its results and its prototype is shown in Figure 5 below.

The simulated and the measured reflection coefficient versus frequency of the antenna are presented in Figure 6 for both bands. The measured $|S_{11}| \leq$ -10 dB illustrates that the antenna achieves a bandwidth of 1.16 GHz (23.16 GHz–24.32 GHz) in the lower band and 634 MHz (28.078 GHz–28.712 GHz) in the upper band. The resonant frequencies were found at 23.52 GHz and 28.39 GHz with a return loss of -43.43 dB and -31.54 dB, respectively. Contrary to the mobile applications, this proposed antenna will exhibit at -6 dB, 3.25 GHz (22.85 GHz–26.10 GHz) in the lower band, and 1.09 GHz (27.87 GHz–28.96 GHz) in the upper band with the same return loss.

The frequency band of 5G technology depends on the region. Table 2 below illustrates that the proposed antenna covers the ISM, radar and 5G frequency bands.

3.2. Gain and efficiency

Being the ability to radiate the received power in any direction compared to a theoretical isotropic antenna, the gain of the proposed antenna is depicted in Figure 7. A system configuration involving two identical antennas placed at 4 cm from each other has been simulated using Ansys HFSS. The transmission coefficient S_{21} was exported to evaluate the antenna gain using the two-antenna method [39] based on the Friis Eq. (8) as given below:

$$G^{(dBi)} = 0.5\left[S_{21}^{dB} + 32.5 + 20\log(fr_{(GHz)}) + 20\log(R_{(m)})\right] \quad (8)$$

where S_{21} is the transmission, f_r the resonant frequency, and R the distance between the two antennas.

In Figure 7, the results show a stable gain of 5.51 dBi in the 24 GHz band and 4.55 dBi in the second band (28 GHz). This illustrates that the angle in which the radiation is constrained is reduced and antenna concentrates its energy towards a specific direction.

From simulation results, the efficiency is 87% and 81%, in the lower and upper band, respectively. Also, by considering the mismatch between the connector, the feedline, and the antenna, the total efficiency is 85% for the 24 GHz band and 68% for the 28 GHz band. This illustrates that the antenna radiates a minimum of 68% of the incident power.

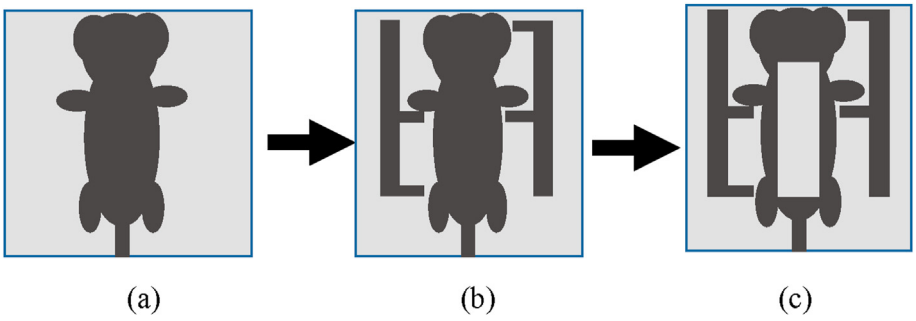

Figure 4. Summarized design process.

Figure 5. Fabricated antenna: (a) top view (b) Bottom view.

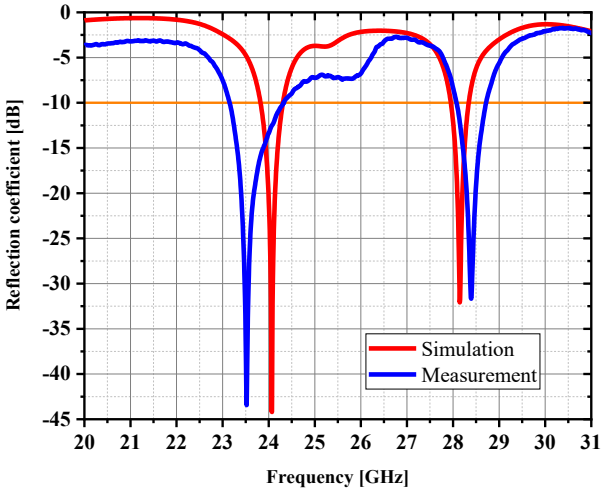

Figure 6. Reflection coefficient of the proposed Dolly-shape antenna.

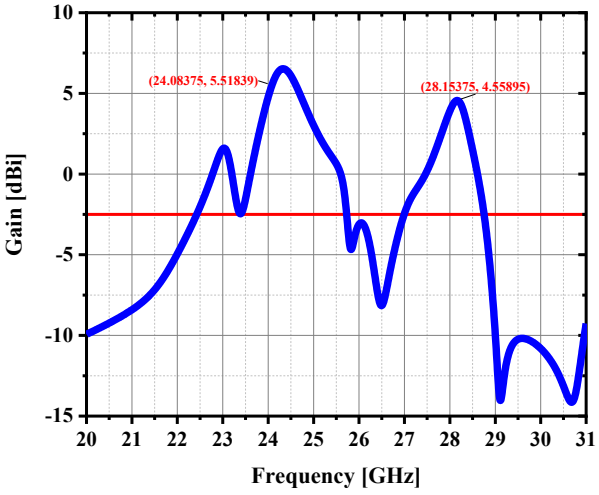

Figure 7. Gain of the proposed DSDBA antenna.

3.3. Current distribution

The surface current distribution gives a better understanding of how the current flows in different antenna compartments at a given frequency. In Figure 8, the current distribution is shown at both resonant frequencies. As it can be noticed, the parasitic elements and rectangular slot played an essential role on both frequency bands in achieving the results.

In the 24 GHz band, the current is more vivid around the feedline's edges, the parasitic elements, the rectangular slot, and the edges of the whole antenna structure's edges with a maximum intensity of 357.7 A/m. The effect of parasitic elements is also observed at 28 GHz, where the surface current distribution seems to be equitable in the upper part of the structure and the feedline while being high toward the edges of the structure, specifically on the armpits of the Dolly-shape. The maximum intensity in the band of 28 GHz is 3639.8 A/m.

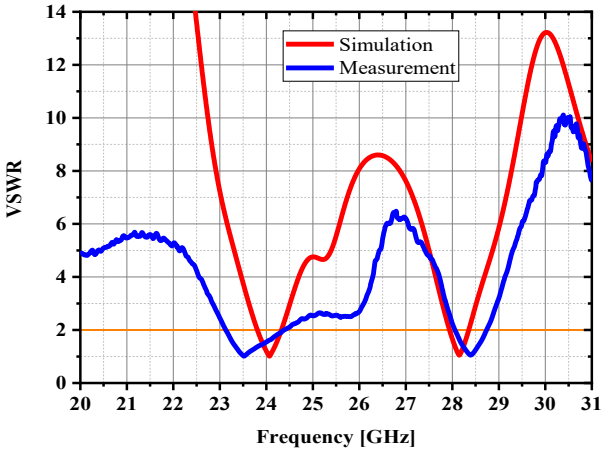

Figure 9. VSWR of the proposed antenna.

3.4. Voltage standing wave ratio and impedance matching

The voltage standing wave ratio (VSWR) indicates the mismatch amount between the antenna and the feedline connected to it. Generally, the value below two is considered as good matching in microwave engineering. Figure 9 presents the impedance matching of the proposed antenna in terms of VSWR. It is observed that the proposed antenna exhibits a maximum VSWR of about 1.05 for both simulation and measurement, as shown in below Figure 9.

The VSWR results plotted in Figure 9 demonstrates that the proposed antenna achieves a good matching across the two operating frequency bands. This implies that a maximum incident power is transferred to the antenna radiating element, which results in 87 % and 81 % radiation efficiency in the lower (24 GHz) and upper (28 GHz) bands, respectively.

The proposed antenna's performance is compared to the previous works on automotive radar and 5G in Table 3.

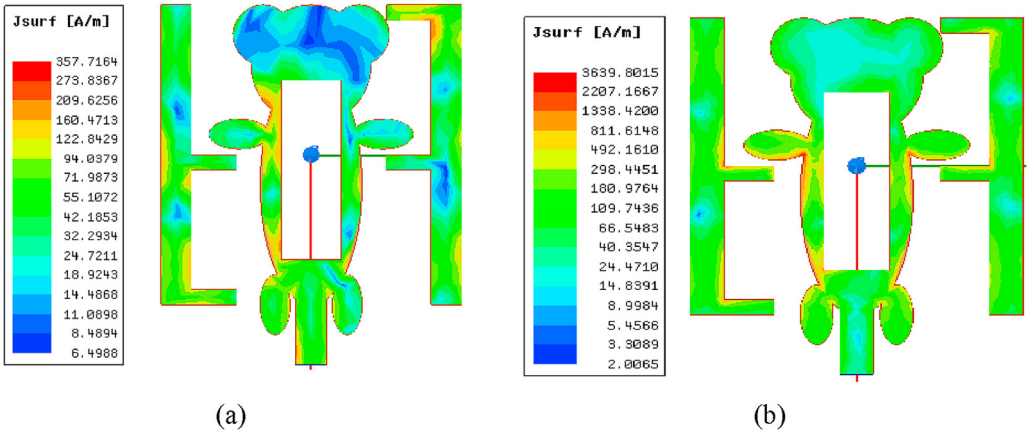

Figure 8. Current distribution of the proposed antenna at 24 GHz (a) and 28 GHz (b).

Table 2. Frequency band for 5G, Short-range radar and ISM band.

Regions	Frequency range				Application
	24–30 GHz	37–50GHz	64–71GHz	>95GHz	
United States of America	24.25–24.45GHz 24.75–25.25GHz 27.5–28.35GHz	37–37.6GHz 37.6–40GHz 47.2–48.2GHz	37–37.6GHz 37.6–40GHz 47.2–48.2GHz	57–64 GHz 64–71 GHz	5G
Canada	26.5–27.5GHz 27.5–28.35GHz	-	37–37.6GHz 37.6–40GHz	57–64 GHz 64–71 GHz	
France	26GHz		57–66GHz		
China	24.75–27.5GHz	40.5–43.5GHz	-	-	
Japan	26.6–27GHz 27–29.5GHz	39–43.5GHz 57–66GHz			
India	24.25–27.5GHz 27.5–29.5GHz	37–43.5GHz			
Australia	24.25–29.5GHz	39GHz	57–66GHz		
United Kingdom	24.5–27.5GHz		57–66GHz		
South Korea	25.7–26.5GHz 26.5–28.9GHz 28.9–29.5GHz	37GHz	57–66GHz		
United States of America	24–24.25 GHz			77–81 GHz	Automotive radars
United States of America	24–24.3 GHz		61.0–61.5 GHz		ISM Application

Table 3. Comparison of the results.

Ref.	Frequency band	Antenna size	Patch area	Gain	Radiation efficiency	Substrate	Substrate thickness	Applications covered
[40]	27.535–28.382 GHz	45.47 mm^2	13.94 mm^2	6.62 dB	70%	Rogers 5880	0.5 mm	5G applications
[41]	27.75–28.77 GHz	361 mm^2	81 mm^2	7.54 dB	62%	Rogers 5880	0.787 mm	5G applications
[5]	27.039–29.199 GHz	243 mm^2	144 mm^2	8.40 dB	83.51%	Duroid RO4003C	0.813 mm	5G applications
[42]	22.60–25.70 GHz	1800 mm^2	400 mm^2	9.7dB	Not provided	FR4	1.6 mm	Radar applications
[43]	23.95–24.53 GHz	792 mm^2	112.68 mm^2	11.9 dB	Not provided	Rogers 4350B	0.254 mm	Radar applications
[44]	27.697–29.33 GHz	36 mm^2	27.17 mm^2	10 dB	98%	RT/Duroid 5880	0.6 mm	5G applications
[45]	24–29.90 GHz	552 mm^2	63.48 mm^2	13.40 dB	98 %	Rogers 5880	0.79 mm	Radar application
[46]	23.89–25.11 GHz	621.62 mm^2	311. 693 mm^2	Not provided	Not provided	Rogers 5880	0.787 mm	Radar application
This work	23.16–24.32 GHz and 28.078–28.712 GHz	49 mm^2	7.053 mm^2	5.51 dBi and 4.55 dBi	87% and 81%	Rogers 3010	1.28 mm	Radar , 5G , and ISM applications

Most of the proposed antennas are focused on either MIMO or Wideband technologies [43, 46]. Moreover, from Table 3, the proposed antenna is the most miniaturized single element antenna that can operate covering simultaneously automotive radar and 5G applications. This is significant because, with an active patch area of 7.053 mm^2 and an overall size of $7 \times 7 \times 1.28$ mm^3, the proposed antenna can easily fit in wireless systems' confined space.

4. Conclusion

This paper proposes the conception and experimental validation of a compact dual-band Dolly-shaped antenna (DBDSA) with a rectangular slot and two F-shaped parasitic elements using microstrip technology. Printed on a $7 \times 7 \times 1.28$ mm^3, which represents an overall electrical size of $0.541\lambda_0 \times 0.541\lambda_0 \times 0.099\lambda_0$, where RO3010 has been used, the DBDSA has a surface area of about 7.053 mm^2. The λ_0 represents the free space wavelength at 23.16 GHz. The radiating element compact size guarantees a -10 dB bandwidth of 1.16 GHz in the range (23.16–24.32) GHz and 634 MHz (28.078–28.712) GHz in the 24 GHz and 28 GHz bands, respectively. It has been pointed out 87% and 81% of the antenna radiation efficiency in automotive radar/ISM band and 5G band, while the in-band gains are 5.51 dBi and 4.55 dBi. The lowest return loss level is approximately -43.43 dB and -31.54 dB in the measurement, which eventually shows the perfect matching of the device in the telecommunication environment. Finally, the DBDSA device is a great and promising candidate for the mix of two leading technologies (radar for automotive and 5G), as experimental results have demonstrated through the prototype measurements. For future work, the design can be used for MIMO and array configurations to increase the data rate and meet other requirements of both 5G and automotive radar applications.

Declarations

Author contribution statement

Ce Lakpo Bamy: Conceived and designed the experiments; Performed the experiments; Analyzed and interpreted the data; Contributed reagents, materials, analysis tools or data; Wrote the paper.

Franck Moukanda Mbango: Analyzed and interpreted the data; Contributed reagents, materials, analysis tools or data.

Dominic Bernard Onyango Konditi: Contributed reagents, materials, analysis tools or data.

Pierre Moukala Mpele: Performed the experiments; Analyzed and interpreted the data; Contributed reagents, materials, analysis tools or data.

Funding statement

This work was supported by the African Union Commission through the Pan African University Institute for Basic Sciences Technology and Innovation (PAUSTI).

Data availability statement

Data included in article/supplementary material/referenced in article.

Declaration of interests statement

The authors declare no conflict of interest.

Additional information

No additional information is available for this paper.

Acknowledgements

The authors would like to acknowledge the contribution of each and every one for the success of this work. An acknowledgement to all the reviewers for their relevant and insightful contributions to advancement of the body of knowledge.

References

[1] M.A. Matin, Review on millimeter wave Antennas-Potential candidate for 5G enabled applications, Adv. Electromagn. 5 (3) (2016) 98–105.
[2] Q. Wu, H. Wang, W. Hong, 'Millimeter-Wave antenna designs', in: Wiley 5G Ref, Wiley, 2019, pp. 1–25.
[3] Huawei, 5G spectrum - public policy position, Publ. Pol. Position (2016) 1–18.
[4] M.H. Sharaf, A.I. Zaki, R.K. Hamad, M.M.M. Omar, A novel dual-band (38/60 GHz) patch antenna for 5G mobile handsets, Sensors 20 (9) (2020) 2541.
[5] S. Kamal, A.S.B. Mohammed, M.F. Bin Ain, et al., A novel negative meander line design of microstrip antenna for 28 GHz mmwave wireless communications, Radio Eng. 29 (3) (2020) 479–485.
[6] M.S. Kamal, M.J. Islam, M.J. Uddin, A.Z.M. Imran, Design of a tri-band microstrip patch antenna for 5G application, Int. Conf. Comput. Commun. Chem. Mater. Electron. Eng. 2018 (2) (2018) 1–3. IC4ME2.
[7] R. Przesmycki, M. Bugaj, L. Nowosielski, Broadband microstrip antenna for 5g wireless systems operating at 28 ghz, Electron 10 (1) (2021) 1–19.
[8] S.X. Ta, H. Choo, I. Park, Broadband printed-dipole antenna and its arrays for 5G applications, IEEE Antenn. Wireless Propag. Lett. 16 (c) (2017) 2183–2186.
[9] Z. Wani, M.P. Abegaonkar, S.K. Koul, A 28-GHz antenna for 5G MIMO applications, Prog. Electromagn. Res. Lett. 78 (December) (2018) 73–79.
[10] Q. Bai, K.L. Ford, R.J. Langley, Switchable electromagnetic bandgap surface wave antenna, Int. J. Antenn. Propag. 2014 (2014) 1–8 (Figure 1).
[11] X. Chen, S. Zhang, Q. Li, A review of mutual coupling in MIMO systems, IEEE Access 6 (2018) 24706–24719.
[12] R.G. Saadallah Alsultan, G.Ö. Yetkin, Mutual coupling reduction of E-shaped MIMO antenna with matrix of C-shaped resonators, Int. J. Antenn. Propag. 2018 (2018).
[13] T.D. Subha, T.D. Subash, K.S. Claudia Jane, D. Devadharshini, D.I. Francis, Study and analysis of suppress of surface wave propagation in microstrip patch antenna, Mater. Today Proc. 24 (2019) 2414–2423.
[14] K.V. Babu, B. Anuradha, Design of multi-band minkowski MIMO antenna to reduce the mutual coupling, J. King Saud Univ. - Eng. Sci. 32 (1) (2020) 51–57.
[15] W. Menzel, Antennas in automobile radar, in: Handbook of Antenna Technologies, Springer Singapore, 2014, pp. 1–22.
[16] M.S. Gupta, Automotive radar, RF Microw. Appl. Syst. (2007) 319–328.
[17] S. Palanivel Rajan, C. Vivek, Analysis and design of microstrip patch antenna for radar communication, J. Electr. Eng. Technol. 14 (2) (2019) 923–929.
[18] J. Gamba, Automotive radar applications, in: Signals and Communication Technology, 2020, pp. 123–142.
[19] M. Tarbouch, A. Elamri, H. Terchoune, Contribution to the miniaturization of antennas: state of the art, Trans. Networks Commun. 4 (5) (2016).
[20] Z. Slavik, O. Bringmann, W. Rosenstiel, Y.C. Eldar, Implications and methods for co-existing automotive radar and communication systems, in: 2018 52nd Asilomar Conference on Signals, Systems, and Computers, IEEE, 2018, pp. 952–956.
[21] V.N. Burov, A.A. Kuzin, A.V. Myakinkov, et al., Development of the automotive radar for the systems of adaptive cruise control and automatic emergency breaking, in: 2019 International Conference on Engineering and Telecommunication (EnT), IEEE, 2019, pp. 1–7.
[22] Y. Jia, Y. Liu, Y. Zhang, A 24 GHz microstrip antenna array with large space and narrow beamwidth, Microw. Opt. Technol. Lett. 62 (4) (2020) 1615–1620.
[23] W. Luo, W. Chen, Y. Feng, Y. Yang, A novel automobile antenna for vehicles communication of IoT systems in 5G network, EURASIP J. Wirel. Commun. Netw. 2020 (1) (2020) 218.
[24] P. Moukala Mpele, F. Moukanda Mbango, D.B.O. Konditi, F. Ndagijimana, A novel quadband ultra miniaturized planar antenna with metallic vias and defected ground structure for portable devices, Heliyon 7 (3) (2021), e06373.
[25] W. Ali, M. Zahid, A. Hussain, U. Kingdom, M.A. Qureshi, Automotive radar and 5G applications, in: Proc. of the 2nd International Conference on Electrical, Communication and Computer Engineering (ICECCE), 2020, pp. 12–13.
[26] M. Awais, A. Riaz, W.T. Khan, An ultra-wideband (16 40 GHz) mmWave antenna for automotive radar and 5G applications, in: 2019 IEEE International Symposium on Antennas and Propagation and USNC-URSI Radio Science Meeting, APSURSI 2019 - Proceedings, IEEE, 2019, pp. 1919–1920.
[27] M. El-Sayed, N. Gad, M. El-Aasser, A. Yahia, Slotted rectangular microstrip-antenna design for radar and 5 G applications, in: Proceedings of 2020 International Conference on Innovative Trends in Communication and Computer Engineering, ITCE 2020, 2020, pp. 330–334.
[28] S.A.R. Parizi, Bandwidth enhancement techniques, in: Trends in Research on Microstrip Antennas, InTech, 2017.
[29] C. Mbinack, B. Bodo, J.S.A. Eyébé Fouda, E. Tonye, Inset-fed rectangular MICROSTRIP patch antenna bandwidth enhancement, Microw. Opt. Technol. Lett. 61 (2) (2019) 562–567.
[30] S. Akinola, I. Hashimu, G. Singh, Gain and bandwidth enhancement techniques of microstrip antenna: a technical review, in: Proc. 2019 Int. Conf. Comput. Intell. Knowl. Econ 2019, ICCIKE, 2019, pp. 175–180.
[31] D.-Z. Zheng, Y. Luo, Q.-X. Chu, Axial-ratio beamwidth and gain enhanced circularly polarized antenna using parasitic elements, Microw. Opt. Technol. Lett. 59 (11) (2017) 2922–2929.
[32] H. Nornikman, B.H. Ahmad, M.Z.A. Abd Aziz, H.A. Bakar, Dual frequencies band and enhanced wideband effect of dual layer microstrip patch antenna with parasitic, J. Phys. Conf. Ser. 1049 (16) (2018), 012012.
[33] Q. Zheng, C. Guo, J. Ding, G.A.E. Vandenbosch, Dual-band metasurface-based CP low-profile patch antenna with parasitic elements, IET Microw., Antennas Propag. 13 (13) (2019) 2360–2364.
[34] G. Kumar, K.P. Ray, Broadband Microstrip Antennas, Artech House, 2003.
[35] P. Moukala Mpele, F. Moukanda Mbango, D.B.O. Konditi, A small dual band (28/38 GHz) elliptical antenna for 5G applications with DGS, Int. J. Sci. Technol. Res. 8 (10) (2019) 353–357.
[36] Y.I.A. Al-Yasir, H.A. Alhamadani, A.S. Kadhim, et al., Design of a wide-band microstrip filtering antenna with modified shaped slots and SIR structure, Inventions 5 (1) (2020) 11.
[37] C.D. Erbas, Parametric analysis of angular rotation for microstrip patch antenna with elliptical patch and parasitic elements, in: 2nd Int. Conf. Electr. Commun. Comput. Eng. 2020, ICECCE, 2020, pp. 12–13.
[38] H.H. Tran, H.C. Park, Gain and bandwidth enhancements of sequential-fed circularly polarized patch antenna array using multiple parasitic elements, Int. J. RF Microw. Comput. Eng. 30 (9) (2020) 1–9.
[39] C.A. Balanis, Antenna Theory : Analysis and Design, fourth ed., Wiley, 2016.
[40] O. Darboe, D.B.O. Konditi, F. Manene, A 28 GHz rectangular microstrip patch antenna for 5G applications, Int. J. Eng. Res. Technol. 12 (6) (2019) 854–857.
[41] Y. Jandi, F. Gharnati, A. Oulad Said, Design of a compact dual bands patch antenna for 5G applications, in: 2017 Int. Conf. Wirel. Technol. Embed. Intell. Syst. 2017, WITS, 2017, pp. 5–8.
[42] Y. Jia, Y. Liu, Y. Zhang, et al., Microstrip array antenna for 24GHz automotive RADAR, IEEE Sensor. J. 62 (21) (2020) 1615–1620.
[43] Y. Jia, Y. Liu, Y. Zhang, et al., In-band RCS reduction and isolation enhancement of a 24 GHz radar antenna using metamaterial absorber for sensing and automotive radar applications, in: 2020 7th Int. Conf. Smart Struct. Syst. ICSSS 2020 20, 2020, pp. 1615–1620.
[44] J. Colaco, R. Lohani, Design and Implementation of microstrip patch antenna for 5G applications, in: Proc. 5th Int. Conf. Commun. Electron. Syst. 2020, ICCES, 2020, pp. 682–685.
[45] S.S. Al-Bawri, M.T. Islam, T. Shabbir, G. Muhammad, M.S. Islam, H.Y. Wong, Hexagonal shaped near zero index (NZI) metamaterial based MIMO antenna for millimeter-wave application, IEEE Access 8 (2020) 181003–181013.
[46] Rusmono, E. Sandi, T. Marani, Design of multiband MIMO antenna for 5G millimeter-wave application, in: IOP Conf. Ser. Mater. Sci. Eng. 852, 2020.